Journal of Power Sources 196 (2011) 6249–6255

Contents lists available at ScienceDirect

Journal of Power Sources

journal homepage: www.elsevier.com/locate/jpowsour

Chloride contamination effects on proton exchange membrane fuel cell performance and durability

Hui Li[a], Haijiang Wang[a,*], Weimin Qian[a], Shengsheng Zhang[a], Silvia Wessel[b], Tommy T.H. Cheng[b], Jun Shen[a], Shaohong Wu[a]

[a] Institute for Fuel Cell Innovation, National Research Council Canada, Vancouver, BC V6T 1W5, Canada
[b] Ballard Power Systems, Inc., Burnaby, BC V5J 5J8, Canada

ARTICLE INFO

Article history:
Received 3 March 2011
Received in revised form 5 April 2011
Accepted 6 April 2011
Available online 12 April 2011

Keywords:
Chlorine contamination
Electrode kinetics
Fuel impurity
Mass transfer
PEM fuel cells

ABSTRACT

Chlorine is a major fuel contaminant when by-product hydrogen from the chlor-alkali industry is used as the fuel for proton exchange membrane (PEM) fuel cells. Understanding the effects of chlorine contamination on fuel cell performance and durability is essential to address fuel cell applications for the automotive and stationary markets. This paper reports our findings of chloride contamination effects on PEM fuel cell performance and durability, as our first step in understanding the effects of chlorine contamination.

Fuel cell contamination tests were conducted by injecting ppm levels of contaminant into the fuel cell from either the fuel stream or the air stream. In situ and ex situ diagnosis were performed to investigate the contamination mechanisms. The results show that cell voltage during chloride contamination is characterized by an initial sudden drop followed by a plateau, regardless of which side the contaminant is introduced into the fuel cell. The drop in cell performance is predominantly due to increased cathode charge transfer resistance as a result of electrochemical catalyst surface area (ECSA) loss attributable to the blocking of active sites by Cl^- and enhanced Pt dissolution.

1. Introduction

Because of their inherent high efficiency, environmental friendliness, and high modularity, polymer electrolyte membrane (PEM) fuel cells are considered to be attractive as power generators for a variety of applications, ranging from transportation [1] to stationary power for buildings and distributed power [2]. Intensive efforts have been made in the last several decades to surmount the challenges that the PEM fuel cell industry has been facing to achieve large-scale commercialization, including high cost and insufficient fuel cell durability. In addition to cost and durability issues, mostly associated with the fuel cell components and in particular the membrane electrode assembly (MEA), the production of high purity hydrogen as well as hydrogen storage and transportation also pose significant technical and cost challenges for large-scale commercialization.

Currently, hydrogen is mostly produced thermochemically from conventional energy sources such as natural gas, gasoline, propane, and methanol through reforming processes (reformate hydrogen) [3]. Hydrogen can also be produced renewably through water electrolysis using energy technologies like solar and wind power (renewably derived hydrogen). Reformate hydrogen often requires an extremely stringent purification process to minimize the concentration of impurities (catalyst poisoning species) that exist inherently due to the reforming processes, such as CO and H_2S, thus increasing the cost of hydrogen production. In addition, if full fuel cycle emissions, including both tailpipe emissions (in the case of transportation applications) and emissions from "upstream" processes (such as feedstock extraction and transport, fuel production, storage, transport, and delivery) are considered, the claim of "zero emissions" for PEM fuel cells based on reformate fuel is not so justified. Renewably derived hydrogen, on the other hand, is a truly "zero emission" fuel but the scarcity of renewable energy dictates its high cost.

In recent years, some fuel cell companies have made efforts to design more robust fuel cell systems that can directly use waste hydrogen from chemical plants as an alternative fuel substitute for reformate hydrogen or electrolytic hydrogen. For example, Ballard Power Systems has recently entered the Distributed Power Generation market using waste hydrogen from chemical plants. In this context, employing alternative hydrogen sources such as waste hydrogen from the chlor-alkali industry is beneficial and cost-effective. The chlor-alkali industry is one of the largest elec-

* Corresponding author at: NRC Institute for Fuel Cell Innovation, 4250 Wesbrook Mall, Vancouver, BC V6T 1W5, Canada. Tel.: +1 604 221 3038; fax: +1 604 221 3001.
E-mail address: haijiang.wang@nrc.gc.ca (H. Wang).

0378-7753/$ – see front matter.
doi:10.1016/j.jpowsour.2011.04.018

trochemical technologies in the world. In 2006, a total of 59 million metric tons of chlorine gas was electrochemically produced and at the same time about 1.7 million tons of hydrogen was generated as a by-product [4]. The hydrogen gas from chlor-alkali cells is normally used to produce hydrochloric acid, burned as a fuel to produce steam, or simply vented to the atmosphere.

Depending on the technology that each chemical plant uses to treat the by-product (or waste) hydrogen, the hydrogen gas normally contains ppm levels of Cl_2 that may negatively impact fuel cell performance if the hydrogen is directly used as the fuel for PEM fuel cells. Therefore, it is of paramount importance to study the effect that chlorine in the hydrogen stream has on PEM fuel cell performance and durability.

Recent studies have examined the adverse effects of chloride in relation to PEM fuel cells. Schmidt et al. [5] and Imabayashi et al. [6] studied the effects of chloride adsorption on the oxygen reduction reaction (ORR) using the rotating ring-disk electrode (RRDE) methodology. They reported that Cl_{ad} acted mainly as a site-blocking species on the Pt surface, and that it was also effective in reducing the number of pairs of Pt sites available for breaking the O–O bond, thus enhancing the formation of H_2O_2 and decreasing the catalytic activity of the catalysts towards the ORR. Yadav et al. [7] studied the effect of Cl^- on the dissolution of electrochemically deposited Pt using electrochemical quartz crystal microbalance (EQCM) and ICP-mass analysis in combination with atomic force microscopy (AFM). The presence of as little as 10 ppm Cl^- resulted in the dissolution of Pt due to the formation of platinum chloride complexes. Some investigations have looked at the poisoning effects of chloride on PEM fuel cell performance and durability through single-cell contamination tests by introducing either HCl or NaCl solution into the cathode air stream [8–11]. Imanura and Ohno [8] and Matsuoka et al. [9] studied the effects of Cl^- by using pumps to directly inject HCl solution into the upstream of the cathode. Cl^- was found to cause significant degradation in cell voltage and loss in ECSAs by promoting Pt dissolution. Similarly, Ali et al. [10] and Steinbach et al. [11] examined the effects of Cl^- by using HCl-containing water in the humidifiers for the air stream, and both found significant but partially recoverable cell performance loss caused by Cl^-.

Although some research work has been published on the contamination effects of Cl^-, as reviewed above, the investigators in all cases introduced HCl or NaCl into the air stream. The introduction of Cl^- into air stream does not reflect how the presence of Cl_2 or Cl^- in the fuel stream would affect fuel cell performance and durability, as in the case of using waste hydrogen from the chlor-alkali industry as the fuel for PEM fuel cells.

In this work, our ultimate goal was to study the effect that chlorine present in the fuel stream has on PEM fuel cell performance and durability. From the chemistry and thermodynamics of chlorine specification [12], it is known that Cl_2, once in contact with water, can easily be converted to HClO, as shown in reaction (1). The highly negative Gibbs free energy for reaction (2) suggests that HClO is highly reducible, particularly in the reducing environment at the anode side of the PEM fuel cell, where both hydrogen and Pt catalysts are present. Therefore, it can be expected that once Cl_2 is introduced into the humidified hydrogen stream and then into the fuel cell anode side, Cl_2, water and hydrogen will undergo reactions (1)–(3), which add up to a total reaction shown in reaction (4).

$$Cl_2(g) + H_2O = HClO + HCl \quad (1)$$

$$HClO + H^+ + 2e^- \rightarrow Cl^- + H_2O; E^\circ = 1.48\,V; \Delta G^\circ = -286\,kJ\,mol^{-1} \quad (2)$$

$$H_2(g) - 2e^- \rightarrow 2H^+; E^\circ = 0.00\,V; \Delta G^\circ = 0.00\,kJ\,mol^{-1} \quad (3)$$

Total reaction:

$$Cl_2(g) + H_2(g) + H_2O \xrightarrow{Pt} 2HCl(aq) + H_2O \quad (4)$$

It can be expected from the above reactions that in the anode environment of the fuel cell, the most dominant Cl species would be Cl^- in the form of HCl, coexisting with lesser amounts of HClO and Cl_2. Although our ultimate goal was to study the effect of chlorine present in the fuel stream, based on the above analysis, as the first step in our series of studies we decided to directly inject equivalent levels of HCl solutions into the hydrogen stream to simulate the effect of introducing Cl_2 into hydrogen. The effects of HClO and Cl_2 will be pursued in future studies.

In this report, we systematically studied the effects of chloride by injecting various levels of HCl into the fuel stream at various current densities, with the aim of understanding the impacts and mechanisms of chlorine contamination. In situ diagnostic techniques employed in this fuel cell performance and durability study included electrochemical impedance spectroscopy (EIS) and cyclic voltammetry (CV). Postmortem diagnostics included inductively coupled plasma (ICP) analysis of the liquid effluents, X-ray diffraction (XRD) analysis of the Pt catalyst particles, as well as scanning electron microscopy (SEM) and energy-dispersive X-ray (EDX) analysis of the contaminated MEA samples.

2. Experimental

2.1. The hardware and MEAs

Teledyne single-cell hardware with gold-coated end plates was employed; the flow-field plates were designed and fabricated in-house using single serpentine channels with 1.2 mm width, 1.0 mm channel depth, and 1.0 mm landing. The MEA consisted of a Gore catalyst coated membrane (CCM) made of PRIMEA® Series 5710 MESGA membrane and two SGL gas diffusion layers (GDLs) with 20% PTFE. The active area of the catalyst layer was 50 cm^2, with 0.4 and 0.1 mg cm^{-2} Pt loadings on the cathode and anode sides, respectively. A fresh MEA was employed for each contamination test.

2.2. Introduction of the contaminant

We have previously reported our studies on the effects of toluene [13], Co^{2+} [14], Al^{3+} and Fe^{3+} [15] in the air stream. The injection unit for the HCl solution in this work was similar to the ones reported in our previous publications, except that the injection unit was installed along the fuel stream tubing between the humidifier and the fuel cell (Fig. 1), instead of alongside the air stream. Because of the corrosive nature of HCl solution, anti-corrosion measures were taken to minimize the potential contamination effects from any other contaminants resulting from HCl corrosion. For example, the high-pressure pump (Smartline Model 100 HP pump) was equipped with a titanium-coated pump head for anti-corrosion protection; polyethylene tubing was used instead of stainless steel tubing to connect the pump to the fuel transfer line through a check valve in order to mitigate potential corrosion of the stainless steel. As well, the polyethylene tubing was extended into the stainless steel tubing that carried the fuel right before the inlet of the fuel cell, to minimize contact between the HCl and the stainless steel tubing.

Since the injection of HCl solution introduced a significant amount of water into the system, the dew point of the hydrogen humidifier was significantly lowered to counterbalance the excess water and to maintain the desired relative humidity (RH) in the fuel cell. Based on the physical chemistry and thermodynamics of mixing water with H_2, the dew point of the H_2 humidifier was cal-

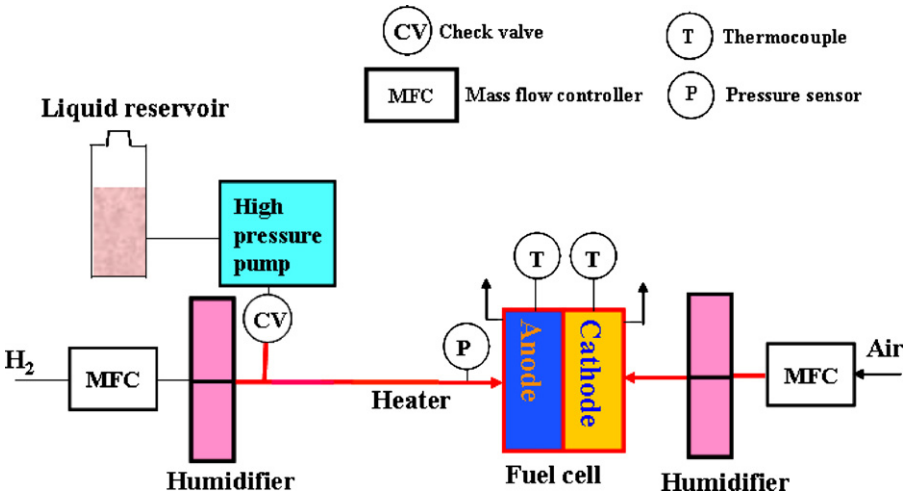

Fig. 1. Schematic of the Cl_2 (HCl) contamination test system.

culated and adjusted during the contamination tests as a function of the fuel cell temperature, fuel cell RH, inlet pressure and the liquid injection rate that determined the HCl (Cl_2) contamination level.

From the results of our diagnostic measurements (EIS and CVs), the injection of HCl solution from the fuel side (anode) resulted in more damage in the cathode catalyst layer (CCL) than in the anode catalyst layer (ACL). As a further step towards understanding the Cl^- contamination mechanisms and to compare the effect of the injection side, air stream contamination tests were also conducted. Consequently a liquid injection unit was installed along the air transfer line in a similar manner to that of the fuel-side injection unit shown in Fig. 1.

2.3. Contamination testing and diagnostic measurements

Using a Fideris 100 W fuel cell test station, contamination tests were conducted in a constant-current discharge mode controlled by a load bank. The contamination effects of various levels of Cl^- were investigated at different current densities under the following conditions: fuel cell temperature: 80 °C; inlet pressure: 25 psig; fuel cell RH: 100%; stoichiometries: 1.5/2.5 H_2/air.

As a diagnostic tool for understanding the contamination mechanisms, EIS measurements were performed at the beginning of test (BOT), middle of test (MOT), and end of test (EOT) using a Solartron 1252 frequency response analyzer (FRA) over the 10k–0.1 Hz range. In addition, CVs were recorded before and after the injection of HCl solution, using a Solartron 1287 potentiostat to evaluate the effect of Cl^- on the ECSA of both anode and cathode catalyst layers. During the CV measurements, the electrode of interest (either cathode or anode) was fed with N_2 while the other electrode was fed with H_2 and acted as the reference electrode.

In addition, physical characterization methods, including SEM, EDX, and XRD were also employed to conduct postmortem analysis on the contaminated CCMs.

3. Results and discussion

3.1. Contamination impacts – fuel cell testing results

3.1.1. Fuel-side injection

The effect of chloride was first studied by injecting HCl into the fuel stream with different contamination levels at various current densities. Fig. 2 shows the fuel cell performance at three levels of HCl (20, 4 and 1 ppm), all at 1.0 A cm^{-2}. Cell performance in the presence of Cl^- displayed a fast, sudden drop, followed by a

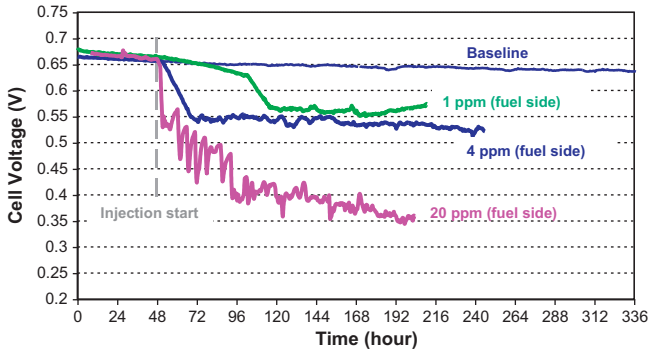

Fig. 2. Contamination testing results at 1.0 A cm^{-2} with fuel-side injection of various levels of HCl. Other operating conditions: fuel cell RH: 100%; fuel cell temperature: 80 °C; stoich: 1.5/2.5 for H_2/air; inlet pressure: 25 psig.

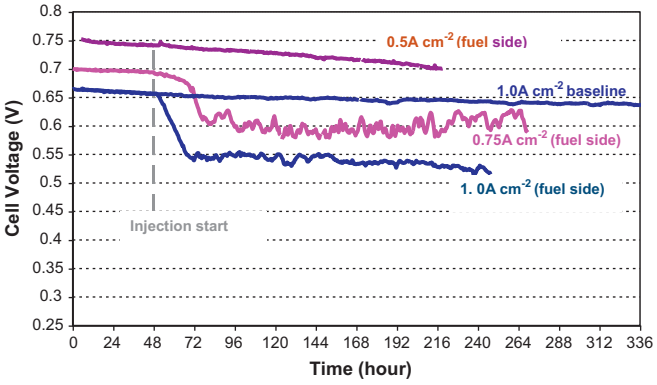

Fig. 3. Contamination testing results with 4 ppm HCl injected from the fuel stream at various current densities. Other operating conditions: fuel cell RH: 100%; fuel cell temperature: 80 °C; stoich: 1.5/2.5 for H_2/air; inlet pressure: 25 psig.

plateau. The "sudden drop" in cell performance was found to be much bigger and occurred earlier at higher HCl concentrations: 120 mV drop for 20 ppm HCl, 106 mV for 4 ppm, and 60 mV for 1 ppm. The fuel cell performance at three current densities (1.0, 0.75 and 0.5 A cm^{-2}) with 4 ppm HCl in the fuel stream is shown in Fig. 3. The presence of 4 ppm of HCl in the fuel side at 0.5 A cm^{-2} resulted in a degradation rate only slightly higher than the baseline in conjunction with the absence of a "sudden drop". However, the presence of 4 ppm HCl at 0.75 and 1.0 A cm^{-2} led to respective "sudden drops" of 92 and 106 mV, indicating that the increase in current

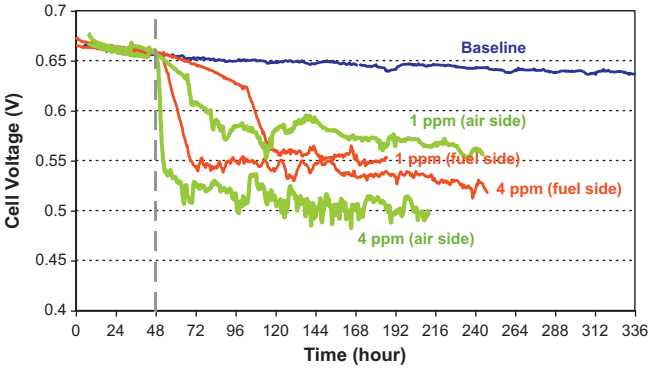

Fig. 4. Comparison of fuel- and air-side injection with two levels of HCl at 1.0 A cm^{-2}. Other operating conditions: fuel cell RH: 100%; fuel cell temperature: 80 °C; stoich: 1.5/2.5 for H_2/air; inlet pressure: 25 psig.

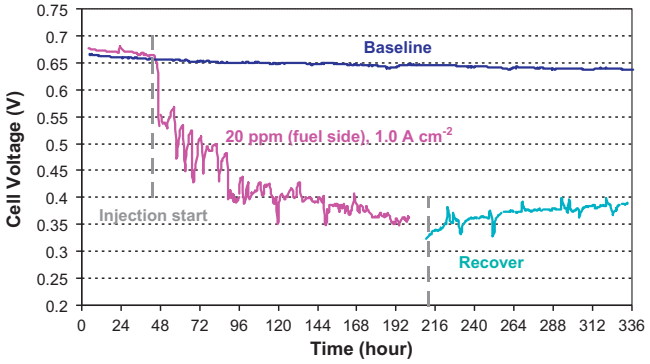

Fig. 5. Recovery tests with 100% humidified H_2 after contamination test with 20 ppm HCl injected from the fuel stream at 1.0 A cm^{-2}. Other operating conditions: fuel cell RH: 100%; fuel cell temperature: 80 °C; stoich: 1.5/2.5 for H_2/air; inlet pressure: 25 psig.

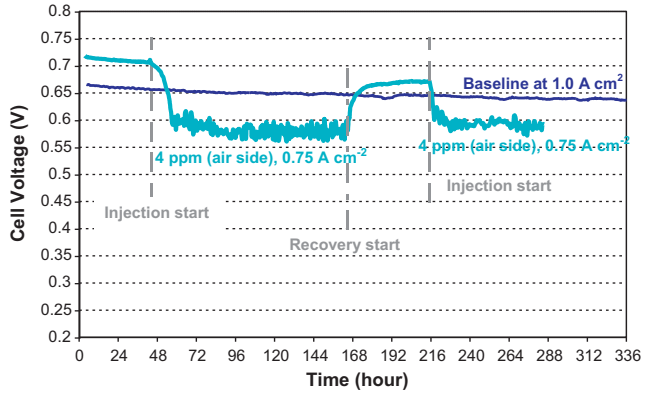

Fig. 6. Recovery tests with 100% humidified H_2 after contamination test with 4 ppm HCl injected from air stream at 0.75 A cm^{-2}, followed by 4 ppm HCl injection at 0.75 A cm^2. Other operating conditions: fuel cell RH: 100%; fuel cell temperature: 80 °C; stoich: 1.5/2.5 for H_2/air; inlet pressure: 25 psig.

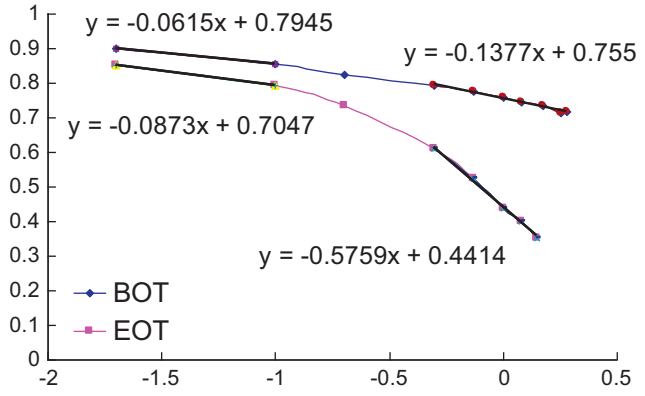

Fig. 7. Polarization curves (IR-free) at both BOT and EOT of the contamination test with 20 ppm HCl at 1.0 A cm^{-2} from fuel-side injection. Other operating conditions: fuel cell RH: 100%; fuel cell temperature: 80 °C; stoich: 1.5/2.5 for H_2/air; inlet pressure: 25 psig.

density enhanced the contamination effect of chloride at the anode side. A possible reason for the different contamination effects at different current densities could be the differences in Cl^- adsorption coverage dictated by cell potential. However, based on results reported by Bagotzky et al. [16] and Zolfaghari et al. [17], at potentials between 0.65 V and 0.75 V (corresponding to the cell potentials of our contamination tests at 1.0 and 0.5 A cm^{-2}) the Cl^- surface adsorption coverage on Pt was found to be almost constant. This suggests that the potential difference among our contamination tests at different current densities would not result in differences in Cl^- adsorption coverage. Therefore, it was more likely that the effect of Cl^- adsorption was exacerbated due to the requirement of more active surface area at higher current densities.

3.1.2. Air-side injection

Fig. 4 compares the effect of injection side (fuel-side injection vs. air-side injection) with two levels of HCl at 1.0 A cm^{-2}. It was found that air-side injection resulted in an earlier and faster "sudden drop" but similar plateau drops (steady-state drops), indicating that regardless of the injection side, Cl^- could cross through the membrane, reaching the other side and causing similar steady-state drops in cell voltage. Comparison of the effect of the injection side will be further discussed in Section 3.2.3 when changes in ECSA are addressed.

3.1.3. Recovery tests

Recovery tests were performed twice by replacing the HCl solution with pure water but maintaining the same liquid injection rate and the same humidifier dew point. The first recovery test was conducted after about 190 h of contamination testing at 1.0 A cm^{-2} with 20 ppm HCl injected from the fuel side (Fig. 5). A second recovery test was conducted after about 190 h of an MEA contaminated at 0.75 A cm^{-2} with 4 ppm HCl injected from the air side, followed by a second period of contamination for about 50 h (Fig. 6). The cell performance was evidently non-recoverable after contamination with 20 ppm Cl^- at 1.0 A cm^{-2}, but was partially recoverable with 4 ppm Cl^- at 0.75 A cm^{-2}. Unfortunately, more systematic tests are needed to draw definite conclusions about recoverability after Cl^- contamination.

3.2. Contamination diagnosis

3.2.1. Polarization curves and OCV changes

Polarization curves were collected at both the BOT and EOT. Fig. 7 shows a representative IR-corrected polarization curve obtained before and after 20 ppm HCl contamination at 1.0 A cm^{-2}. The Tafel slope at a lower current density increased from 0.062 to 0.087 V decade^{-1} and the exchange current density decreased due to Cl^- contamination. The shift in Tafel slope concurred with the notion that H_2O_2 was enhanced in the presence of Cl^-. In addition, the Tafel slope at the higher current density was found to be six times that at the lower current density due to the contamination, whereas it would have only doubled in the case without contamination. Furthermore, it was also observed that the increase in contamination level enhanced the degradation effect of Cl^- on fuel cell performance, in both the kinetic region and the mass trans-

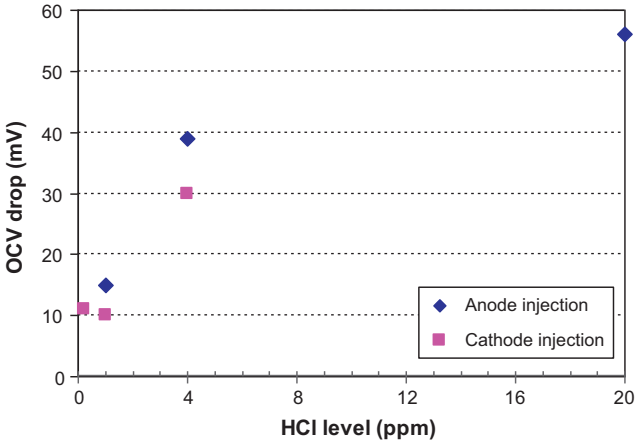

Fig. 8. Change in OCV as a function of HCl concentration for contamination tests conducted at 1.0 A cm^{-2}. Other operating conditions: fuel cell RH: 100%; fuel cell temperature: 80 °C; stoich: 1.5/2.5 for H_2/air; inlet pressure: 25 psig.

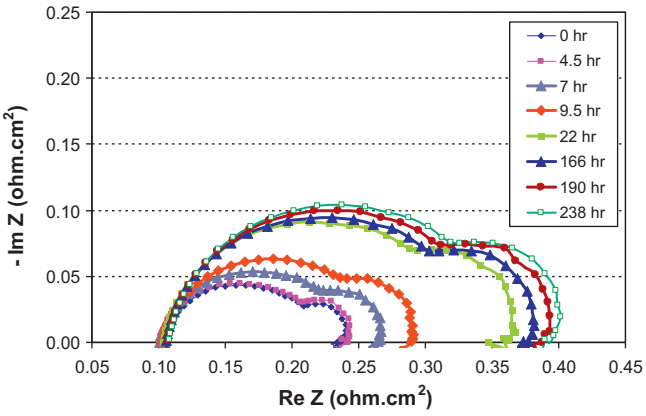

Fig. 9. Nyquist plots vs. time for contamination test at 1.0 A cm^{-2} with 4 ppm HCl from fuel-side injection. Other operating conditions: fuel cell RH: 100%; fuel cell temperature: 80 °C; stoich: 1.5/2.5 for H_2/air; inlet pressure: 25 psig.

port region. Similar observations were made for all other tests. The effect of Cl^- on the kinetics was most likely due to Cl^- adsorption blocking the catalyst active sites and the promotion of H_2O_2 production, as also reported by Schmidt et al. [5] and Imabayashi et al. [6]. On the other hand, the effect of Cl^- on mass transport might be related to Cl^- adsorption on the C support which changed the surface structure and/or hydrophobicity of the catalyst layer.

In addition to the effect on the steady-state polarization curve, the presence of Cl^-, whether injected from the air or the fuel side, also resulted in decreases in OCV. Fig. 8 illustrates the reduction in OCV at 1.0 A cm^{-2} as a function of Cl^- level from both air- and fuel-side injections. The reduction of OCV followed the same trend, regardless of the injection side, again supporting the Cl^- crossover phenomenon.

3.2.2. EIS

EIS was collected at the BOT, MOT, and EOT. A typical set of Nyquist plots for the contamination test conducted with 4 ppm HCl at 1.0 A cm^{-2} from fuel-side injection is shown in Fig. 9. To distinguish which part of the fuel cell process (charge transfer, mass transfer, or membrane conduction) was most affected by Cl^- contamination; the numerical data for the three individual resistances were fitted as a function of contamination time using the equivalent circuit reported in our previous publication [18]. For all of our contamination tests, the increase in charge transfer resistance was the dominant contributor to the total resistance increase (in

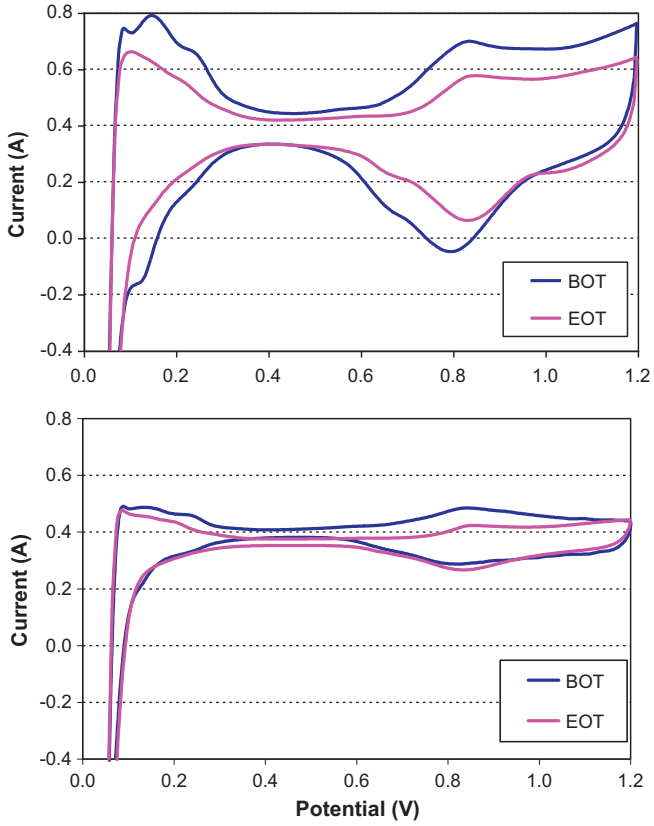

Fig. 10. Cathode and anode CVs for contamination test at 1.0 A cm^{-2} with 4 ppm HCl from fuel-side injection. Other operating conditions: fuel cell RH: 100%; fuel cell temperature: 80 °C; stoich: 1.5/2.5 for H_2/air; inlet pressure: 25 psig.

the case shown in Fig. 9, the increase in charge transfer resistance contributed about 75% of the increase in total resistance due to the contamination effect of 4 ppm HCl in the fuel stream at 1.0 A cm^{-2}).

3.2.3. CVs and ECSAs

Cathode and anode side CVs were recorded at both the BOT and EOT of the contamination tests, and the corresponding ECSAs were calculated from the hydrogen desorption and adsorption peaks in those CVs. Two observations can be made about the cathode side CV (a typical cathode and anode CV set before and after contamination is shown in Fig. 10):

(1) The H_2 desorption and adsorption peaks were significantly reduced as a result of Cl^- contamination. This was in agreement with what was reported by Bagotzky et al. [16], who experimentally studied the effect of Cl^- specific adsorption on the adsorption of hydrogen on the Pt surface. They concluded that practically no hydrogen adsorption occurred on a Pt surface covered by a monolayer of adsorbed Cl^-, due to the decreased H–Pt bond energy. In other words, the specifically adsorbed Cl^- on the Pt surface essentially acted as a blocking agent, thus reducing the ECSA. In addition to the site-blocking effect of Cl^- on the Pt surface, enhanced Pt dissolution in the presence of Cl^- could be another reason for the reduced ECSA, as reported by Yadav et al. [7]. They experimentally confirmed that Pt dissolution could be accelerated by the electrochemical formation of chloride complexes in chloride-containing solutions through the following reactions:

$$Pt + 4Cl^- \rightarrow PtCl_4^{2-} + 2e^- \quad (5)$$

$$Pt + 6Cl^- \rightarrow PtCl_6^{2-} + 4e^- \quad (6)$$

(2) The Pt/PtO redox peaks were also reduced as a result of contamination. Yadav et al. [7] examined the effect of Cl^- on Pt oxide

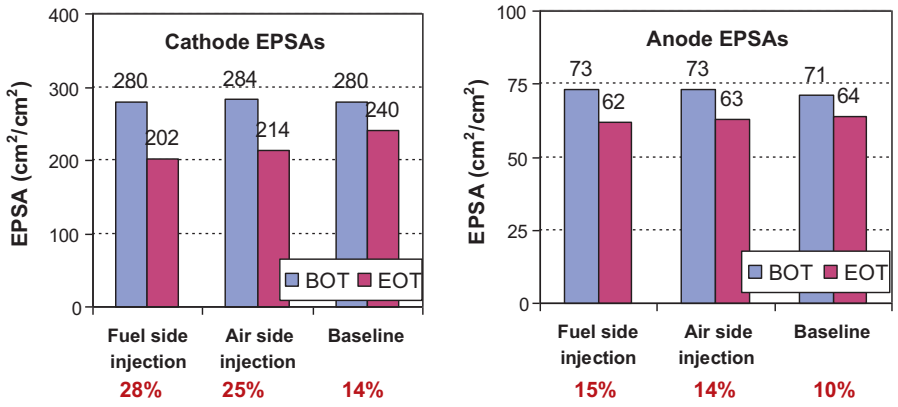

Fig. 11. Cathode and anode ECSAs for contamination tests conducted at 1.0 A cm^{-2} with 1.0 ppm Cl$^-$ from either fuel-side or air-side injection, in comparison with baseline ECSAs. The percentages in the figure are the reduction in ECSAs from original values. Other operating conditions: fuel cell RH: 100%; fuel cell temperature: 80 °C; stoich: 1.5/2.5 for H_2/air; inlet pressure: 25 psig. *Note*: the testing times for the two contamination tests and one baseline test are 238, 240 and 240 h, respectively.

formation and reported that the adsorbed Cl$^-$ on the Pt surface caused a strong retardation of Pt oxide formation, which agreed with the reduced Pt oxidation peak observed during the forward scan in Fig. 10. The reduced Pt oxide reduction peak during the backward scan in Fig. 10 was also a demonstration of reduced oxide formation in the presence of Cl$^-$ adsorption. It should be mentioned that in some cases the double-layer region (from 0.4 to 0.75 V in the voltammogram) widened, which might be caused by the presence of Cl$^-$ in the catalyst–electrolyte interface.

Similar observations were observed for the anode CVs in Fig. 10, except that the reduction of both the H adsorption/desorption peaks and the Pt/PtO redox peaks was found to be more pronounced on the cathode side, even though the 4 ppm HCl was injected from the fuel side. This is demonstrated more clearly in Fig. 11, which compares the ECSAs at BOT and EOT, i.e. with and without 1 ppm HCl injection from either the air side or the fuel side. Regardless of the injection side, 1 ppm HCl resulted in more ECSA reduction in the cathode catalyst layer than in the anode catalyst layer; the cathode and anode ECSAs were reduced by 28% and 15%, respectively, with fuel-side injection, and by 25% and 14%, respectively, with air-side injection. This further confirmed that Cl$^-$ could migrate from the anode to the cathode side when injected into the fuel stream, causing more reduction in the cathode ECSA than in the anode ECSA. The crossover of Cl$^-$ through the membrane was also examined using ICP elemental analysis conducted with the effluents collected from the anode and cathode outlets of the fuel cell during the contamination tests. Regardless of the injection side, Cl$^-$ was detected in the effluents collected from both fuel cell outlets.

The reduction in cathode ECSAs was also plotted against the level of contaminant Cl$^-$ for all the tests conducted at 1.0 A cm^{-2}, including tests with both air- and fuel-side injection (Fig. 12). Clearly, regardless of the injection side, the reduction in cathode ECSA followed the same relationship with the Cl$^-$ contamination level.

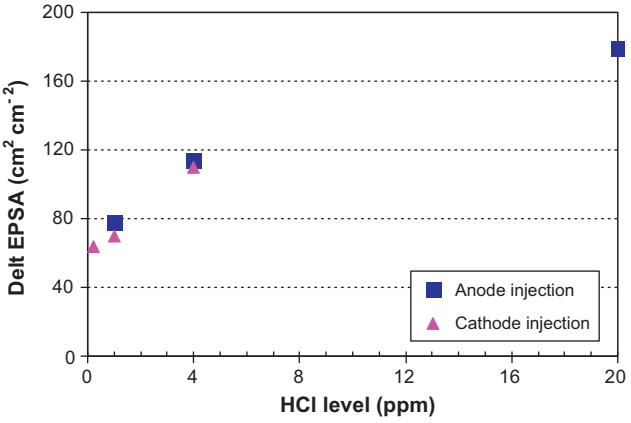

Fig. 12. Reduction of cathode ECSA vs. Cl$^-$ level for contamination tests conducted at 1.0 A cm^{-2} with either air-side or fuel-side injection. Other operating conditions: fuel cell RH: 100%; fuel cell temperature: 80 °C; stoich: 1.5/2.5 for H_2/air; inlet pressure: 25 psig.

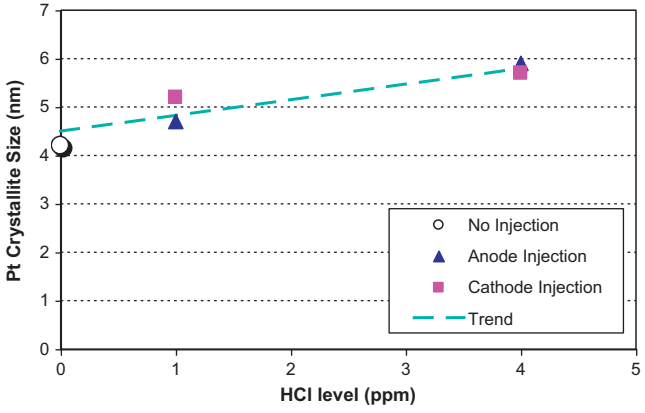

Fig. 13. XRD analysis results: EOT cathode Pt crystallite size vs. Cl$^-$ contamination level, obtained from contamination tests conducted at 1.0 A cm^{-2} with both air-side and fuel-side injection.

3.2.4. SEM, EDX and XRD analysis

SEM imaging and EDX elemental analysis were conducted with some of the MEAs that had been subjected to contamination tests with HCl solution injected from the fuel or air streams, to examine the effect of HCl contamination on the CCM component thickness, and determine whether Cl$^-$ was present in the respective CCM components, including the CCL, ACL and polymer exchange membrane. The SEM images revealed that the changes in the thicknesses of all three CCM layers were insignificant. With respect to Cl$^-$ analysis, the EDX line scans (Table 1) showed that Cl$^-$ was detected in both the CCL and ACL but not in the membrane of the three CCMs subjected to HCl contamination tests injected through the fuel side. This again confirmed the crossover of Cl$^-$ through the membrane.

To examine whether Cl$^-$ contamination resulted in changes in Pt particle size, cathode catalyst particles were scraped off the contaminated CCMs for XRD analysis. Fig. 13 shows the EOT cathode Pt crystallite size (calculated from six XRD spectra) as a function of Cl$^-$ contamination level, obtained from contamination tests con-

Table 1
Cl^- content in CCM components (unit: at.%).

CCL			ACL			Membrane		
CCM 1[a]	CCM 2[a]	CCM 3[a]	CCM 1	CCM 2	CCM 3	CCM 1	CCM 2	CCM 3
1.52	0.62	0.56	0.97	1.61	1.16	ND[b]	ND	ND

[a] CCMs 1–3 refer to MEAs subjected to contamination tests with 20 ppm HCl at 1.0 A cm^{-2} for 144 h, 4 ppm HCl at 1.0 A cm^{-2} for 238 h, and 4 ppm HCl at 0.5 A cm^{-2} for 171 h, respectively, all from fuel-side injection.
[b] Not detected.

ducted at 1.0 A cm^{-2}. Pt particle size increased as a result of Cl^- contamination, and the degree of increase was proportional to the Cl^- contamination level, regardless of whether the Cl^- was injected into the fuel cell from the anode or the cathode side. This increase was explained by enhanced Pt dissolution in the presence of Cl^-, as discussed earlier.

4. Conclusions

The presence of trace levels of Cl_2 has been identified as an impurity in the waste hydrogen produced from the chloro-alkaline industry that could potentially be used as a fuel for PEM fuel cells. The effects of Cl_2 on PEM fuel cell performance and durability were studied by separately injecting solutions of various HCl concentrations into the fuel stream and the air stream. When Cl^- was present in either the fuel stream or the air stream, the cell performance measured by cell voltage at a constant current density was characterized by an initial sudden decline, followed by a steady-state drop (plateau). The severity of the contamination effect was found to be independent of the injection side but to increase with both current density and HCl concentration.

Preliminary recovery tests revealed that cell performance was non-recoverable in some cases, such as with high Cl^- concentrations, but partially recoverable with a low level of Cl^-. More work is needed to study recoverability after Cl^- contamination.

EIS measurements indicated that contamination resulted in an increase in both the charge transfer and mass transfer resistances on the cathode side, but the increase in kinetic resistance was the dominant contributor to the cell performance loss. Regardless of the injection side, the presence of Cl^- caused a more significant decrease in cathode ECSA than anode ECSA. The reduction in ECSA was explained as the result of both the site-blocking effect of specifically adsorbed Cl^- on the Pt surface and the enhancement of Pt dissolution by the electrochemical formation of chloride complexes. The EOT cathode Pt crystallite size, determined by XRD, was found to increase with Cl^- concentration irrespective of injection in the fuel or air streams.

This research is important for understanding the contamination mechanism of chlorine and its effect on fuel cell performance and the development of mitigation strategies to handle fuel cell contamination if waste hydrogen produced by the chloro-alkali industry is to be used as fuel for PEM fuel cells.

Acknowledgments

The authors gratefully acknowledge financial support from the Institute for Fuel Cell Innovation of the National Research Council of Canada (NRC-IFCI) and Ballard Power Systems Inc. The authors also acknowledge the funding provided by Natural Resources Canada through the Clean Energy Fund, a component of the Government of Canada's Economic Action Plan.

References

[1] R. Shimoi, T. Aoyama, A. Iiyama, SAE World Congress, Fuel Cell Vehicle Applications Session, SP-2236, April 20–23, Detroit, USA (2009) 105–115.
[2] T. Susai, A. Kawakami, A. Hamada, Y. Miyake, Y. Azegami, J. Power Sources 92 (2002) 131–138.
[3] A.F. Ghenciu, Curr. Opin. Solid State Mater. Sci. 6 (2002) 389–399.
[4] T.V. Bommaraju, Paul J. Orosz, and Elizabeth A. Sokol, Brine Electrolysis Electrochemistry Encyclopaedia, September 2007, http://electrochem.cwru.edu/encycl/art-b01-brine.htm. accessed 21 April. 2011.
[5] T.J. Schmidt, U.A. Paulus, H.A. Gasteiger, R.J. Behm, J. Electrochem. Chem. 508 (2001) 41–47.
[6] S. Imabayashi, Y. Kondo, R. Komori, A. Kawano, J. Ohsaka, ECS Trans. 16 (2) (2008) 925–930.
[7] A.P. Yadav, A. Nishikata, T. Tsuru, Electrochim. Acta 52 (2007) 7444–7452.
[8] D. Imamura, K. Ohno, Fuel Cell Seminar & Exposition: Fuel Cells, 2009, LRD 25–49.
[9] K. Matsuoka, S. Sakamoto, K. Nakato, A. Hamada, Y. Itoh, J. Power Sources 179 (2008) 560–565.
[10] S.T. Ali, Q. Li, C. Pan, J.O. Jensen, L.P. Nielsen, Int. J. Hydrogen Energy 36 (2011) 1628–1636.
[11] A.J. Steinbach, C.V. Hamilton, M.K. Debe, ECS Trans. 11 (1) (2007) 889–902.
[12] V.V. Rajasekharan, B.N. Clark, S. Boonsalee, J.A. Switzer, Environ. Sci. Technol. 41 (2007) 4252–4257.
[13] H. Li, J.L. Zhang, Z. Shi, D. Song, K. Fatih, S. Wu, H. Wang, J.J. Zhang, N. Jia, S. Wessel, R. Abouatallah, N. Joos, J. Electrochem. Soc. 156 (2) (2009) B252–B257.
[14] H. Li, J. Gazzarri, K. Tsay, S. Wu, H. Wang, J.J. Zhang, S. Wessel, R. Abouatallah, N. Joos, J. Schrooten, Electrochim. Acta 54 (2010) 5823–5830.
[15] H. Li, K. Tsay, H. Wang, J. Shen, S. Wu, J.J. Zahng, N. Jia, S. Wessel, R. Abouatallah, N. Joos, J. Schrooten, J. Power Sources 195 (2010) 8089–8093.
[16] V.S. Bagotzky, Y.B. Vassilyev, J. Weber, J.N. Pirtskhalava, J. Electroanal. Chem. 27 (1970) 31–46.
[17] A. Zolfaghari, B.E. Conway, G. Jerkiewicz, Electrochim. Acta 47 (2002) 1173–1187.
[18] H. Li, J.L. Zhang, K. Fatih, Z. Wang, Y. Tang, Z. Shi, S. Wu, D. Song, J.J. Zhang, N. Jia, S. Wessel, R. Abouatallah, N. Joos, J. Power Sources 185 (2008) 272–279.